AN EFFICIENT BOUNDARY MESHFREE COMPUTATIONAL APPROACH FOR 3-D MULTI-DOMAIN TRANSIENT THERMAL ANALYSIS WITH VARIABLE THERMAL SOURCES IN NON-HOMOGENEOUS MEDIA

by

Jing LING, Dong-Sheng YANG*, Hong-Ying WANG, and Hong-Zhong MOU

School of Materials and Architectural Engineering (Guizhou School of Emergency Management), Guizhou Normal University, Guiyang, China

Original scientific paper
https://doi.org/10.2298/TSCI TSCI230215099L

Solutions of 3-D multi-domain transient thermal analysis with variable thermal sources in non-homogeneous media are separated into homogeneous and special solutions by an efficient boundary meshfree computational approach, namely virtual boundary meshfree Galerkin method. Homogeneous solutions are expressed by the virtual boundary element method. The virtual source functions of homogeneous solutions and the unknowable coefficients of special solutions can be formed by the radial basis function interpolation. Considering the control equation, the boundary and continuous conditions, and using the Galerkin method, the discrete formula for 3-D multi-domain transient thermal analysis with variable thermal sources in non-homogeneous media can be obtained. This discrete equation has symmetry. Meanwhile, in order to illustrate the steps of implementation more clearly, the final detailed implementation process is given. The numerical results of two calculation examples are obtained and compared to other methods and exact solutions. The proposed method's stability and exactness are validated for 3-D multi-domain transient thermal analysis with variable thermal sources in non-homogeneous media.

Key words*: 3-D transient thermal non-homogeneous media, meshfree method, variable thermal source, multi-domain, boundary element method*

Introduction

Thermal conduction problems are a very important class of problems in engineering and scientific research [1, 2]. In fact, many thermal conduction problems are transient thermal conduction problems varying with time, such as the cutting thermal conduction of steel [3], the metal welding [4], the rocket engine [5], and so forth. The boundary element method has semi analytical and semi numerical characteristics. It is a prominent technique to calculate these kind of transient thermal conduction problems, especially 3-D problems. Such as Fu *et al.* [6] analysed the transient anomalous thermal conductions in functionally graded materials with the help of the singular boundary collocation method. Jiang *et al.* [7] used boundary element method (BEM) with the radial integration and the modified Levenberg-Marquardt approach to solve the shape reconstruction of transient thermal conduction problems. Yu *et al.* [8, 9] computed 3-D functionally graded materials of transient thermal conduction problems with the help of the isogeometric dual reciprocity BEM. Jacinto *et al.* [10] calculated the transient thermal conduction of the heterogeneous solid medium by combining BEM and analytical solutions. Xu *et al.* [11] utilized the isogeometric BEM to analyze the functionally graded materials with

* Corresponding author, e-mail: yds415@gznu.edu.cn

the transient thermal conduction problems. There are some advantages to the aforementioned BEM, but they also have some drawbacks. These include the singular integral, the vertex question, the boundary-layer effect, and so forth.

Virtual BEM [12, 13] can eliminate these mentioned defects. It is assumed that the point loads exist on the virtual boundaries [12]. Subsequently, the continuous virtual source functions are used instead of point loads [13, 14] to enhance the computational exactness. Combining the meshfree method and VBEM, the virtual source functions are interpolated with the help of the moving least squares approximation [15] in order to make better the calculation exactness. However, the weighting coefficients are artificially set [15]. To get the unique weighting coefficients, considering the Galerkin method, the meshfree method, and VBEM, the virtual boundary meshfree Galerkin method (VBMGM) is formed for 2-D single-domain thermal conduction problems with thermal sources [16]. The coefficient matrix of VBMGM is sparse and symmetric. Since the calculation problems of thermal conductions are often composed of different materials, an effective way to calculate the thermal conduction problems is to use the multi-domain combination method. The VBMGM as an efficient boundary meshfree computational approach is extended to 3-D multi-domain transient thermal analysis with variable thermal sources in non-homogeneous media.

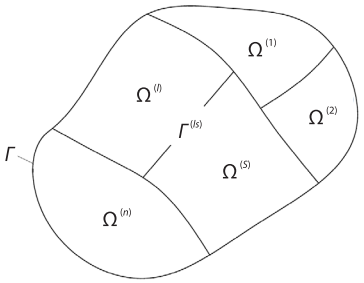

Figure 1. Schematic diagram of multi-domain combinatorial problems

Mathematical formulation

The relationship between the whole domain and subdomains of the multi-domain transient thermal analysis is shown in fig. 1. The whole domain Ω is composed of subdomains [13]. Take the l^{th} sub domain $\Omega^{(l)}$ as an example to illustrate the relationship between subdomains and the whole domain Ω. The $\Omega = \Omega^{(1)} \cup \Omega^{(2)} \cup ... \Omega^{(l)} ... \cup \Omega^{(n)}$ and $\Omega^{(1)} \cap \Omega^{(2)} \cap ... \Omega^{(l)} ... \cap \Omega^{(n)} = \varnothing$ (the null set). The real boundaries of the whole domain Ω and the l^{th} subdomain $\Omega^{(l)}$ are recorded as Γ and $\Gamma^{(l)}$, respectively. Suppose that the l^{th} and sth subdomains share the common or continuous boundary, namely $\Gamma^{(ls)}$.

The control equation is given for the transient thermal analysis with variable thermal sources in non-homogeneous media in the l subdomain $\Omega^{(l)}$:

$$\begin{aligned} &\nabla\left[k^{(l)}(\boldsymbol{x})\nabla T^{(l)}(\boldsymbol{x},t)\right]+Q^{(l)}(\boldsymbol{x},t)= \\ &=\nabla k^{(l)}(\boldsymbol{x})\nabla T^{(l)}(\boldsymbol{x},t)+k^{(l)}(\boldsymbol{x})\nabla^2 T^{(l)}(\boldsymbol{x},t)+Q^{(l)}(\boldsymbol{x},t)= \\ &=\rho^{(l)}(\boldsymbol{x})c^{(l)}(\boldsymbol{x})\frac{\partial T^{(l)}(\boldsymbol{x},t)}{\partial t}, \quad \boldsymbol{x}\in\Omega^{(l)} \end{aligned} \tag{1}$$

where $k^{(l)}(\boldsymbol{x})$, $c^{(l)}(\boldsymbol{x})$, and $\rho^{(l)}(\boldsymbol{x})$ are the thermal conductivity coefficient, the specific thermal capacity and the density of the subdomain $\Omega^{(l)}$, respectively, ∇ is the Laplace operator, $T^{(l)}(\boldsymbol{x}, t)$ and $Q^{(l)}(\boldsymbol{x}, t)$ are the temperature and the thermal source on the $\boldsymbol{x}$ point at time, t, respectively, and ∂ represents the partial derivative.

The $T^{(l)}(\boldsymbol{x}, t)$ and $Q^{(l)}(\boldsymbol{x}, t)$ in eq. (1) can be demonstrated by the time step difference scheme with full implicitness, namely $T^{(l)}(\boldsymbol{x}, t) = T^{(l)}_{t+\Delta t}(\boldsymbol{x})$, $Q^{(l)}(\boldsymbol{x}, t) = Q^{(l)}_{t+\Delta t}(\boldsymbol{x})$, and $\partial T^{(l)}(\boldsymbol{x}, t)/\partial t \approx [T^{(l)}_{t+\Delta t}(\boldsymbol{x}) - \partial T^{(l)}_t(\boldsymbol{x})]/\Delta t$, where Δt is the time step. The $T^{(l)}_t(\boldsymbol{x})$, $Q^{(l)}_t(\boldsymbol{x})$, $T^{(l)}_{t+\Delta t}(\boldsymbol{x})$, and $Q^{(l)}_{t+\Delta t}(\boldsymbol{x})$ are the computed temperature and thermal source on the $\boldsymbol{x}$ point at t and $t + \Delta t$ time, respectively. Then, eq. (1) can be changed:

$$\nabla k^{(l)}(\boldsymbol{x})\nabla T^{(l)}_{t+\Delta t}(\boldsymbol{x})+k^{(l)}(\boldsymbol{x})\nabla^2 T^{(l)}_{t+\Delta t}(\boldsymbol{x})+Q^{(l)}_{t+\Delta t}(\boldsymbol{x})-\frac{\rho^{(l)}c^{(l)}T^{(l)}_{t+\Delta t}(\boldsymbol{x})}{\Delta t}= =\frac{-\rho^{(l)}c^{(l)}T^{(l)}_{l}(\boldsymbol{x})}{\Delta t},\ \ \boldsymbol{x}\in\Omega^{(l)} \tag{2}$$

The thermal source, boundary and continuous conditions at $t + t\Delta$ time for the l subdomain of 3-D transient thermal analysis can be given:

$$Q^{(l)}_{t+\Delta t}(\boldsymbol{x})=\bar{Q}^{(l)}_{t+\Delta t}(\boldsymbol{x}),\ \ \boldsymbol{x}\in\Omega^{(l)} \tag{3}$$

$$T^{(l)}_{t+\Delta t}(\boldsymbol{x})=\bar{T}^{(l)}_{t+\Delta t}(\boldsymbol{x}),\ \ \boldsymbol{x}\in\Gamma^{(l)}_{T} \tag{4}$$

$$q^{(l)}_{t+\Delta t}(\boldsymbol{x})=\bar{q}^{(l)}_{t+\Delta t}(\boldsymbol{x}),\ \ \boldsymbol{x}\in\Gamma^{(l)}_{q} \tag{5}$$

$$T^{(l)}_{t+\Delta t}(\boldsymbol{x})=T^{(s)}_{t+\Delta t}(\boldsymbol{x}),\ \ \boldsymbol{x}\in\Gamma^{(ls)} \tag{6}$$

$$q^{(l)}_{t+\Delta t}(\boldsymbol{x})=-q^{(s)}_{t+\Delta t}(\boldsymbol{x}),\ \ \boldsymbol{x}\in\Gamma^{(ls)} \tag{7}$$

where $\bar{Q}^{(l)}_{t+\Delta t}(\boldsymbol{x})$ is the known thermal source within the lth subdomain $\Omega^{(l)}$, $\bar{T}^{(l)}_{t+\Delta t}(\boldsymbol{x})$ and $\bar{q}^{(l)}_{t+\Delta t}(\boldsymbol{x})$ are the values of temperature and thermal flux on the boundary $\Gamma^{(l)}_{T}$ with the known temperature and the boundary $\Gamma^{(l)}_{q}$ with known thermal flux in $\Omega^{(l)}$, respectively.

Considering that eq. (2) is a non-homogeneous equation, $\bar{T}^{(l)}_{t+\Delta t}(\boldsymbol{x})$ is composed of the homogeneous solution $\bar{T}^{(l)hs}_{t+\Delta t}(\boldsymbol{x})$ and special solution $\bar{T}^{(l)ss}_{t+\Delta t}(\boldsymbol{x})$:

$$T^{(l)}_{t+\Delta t}(\boldsymbol{x})=T^{(l)hs}_{t+\Delta t}(\boldsymbol{x})+T^{(l)ss}_{t+\Delta t}(\boldsymbol{x}) \tag{8}$$

Because of $q^{(l)}_{t+\Delta t}(\boldsymbol{x}) = -k^{(l)}\partial T^{(l)}_{t+\Delta t}(\boldsymbol{x})/\partial n$, $q^{(l)}_{t+\Delta t}(\boldsymbol{x})$ is also made up of the homogeneous solution $q^{(l)hs}_{t+\Delta t}(\boldsymbol{x})$ and special solution $q^{(l)ss}_{t+\Delta t}(\boldsymbol{x})$:

$$q^{(l)}_{t+\Delta t}(\boldsymbol{x})=q^{(l)hs}_{t+\Delta t}(\boldsymbol{x})+q^{(l)ss}_{t+\Delta t}(\boldsymbol{x}) \tag{9}$$

Solution algorithm

Homogeneous solutions

The homogeneous solutions $T^{(l)hs}_{t+\Delta t}(\boldsymbol{x})$ and $q^{(l)hs}_{t+\Delta t}(\boldsymbol{x})$ are demonstrated by VBEM [17]. Next, VBEM of any 3-D subdomain is introduced. The boundary $\Gamma^{(l)}$ of the l^{th} subdomain $\Omega^{(l)}$ can be extended along the normal outward direction $n(\boldsymbol{x})$ of any point $\boldsymbol{x}$ in fig. 2. The virtual subdomain and its virtual boundary are recorded as $\Omega^{(l)\prime}$ and $S^{(l)}$, respectively. The continuous virtual source function $\varphi^{(l)}_{t+\Delta t}(\boldsymbol{\xi})$ exists at any point $\boldsymbol{\xi}$ of the virtual boundary $S^{(l)}$.

The $\varphi^{(l)}_{t+\Delta t}(\boldsymbol{\xi})$ is interpolated by the radial basis function interpolation (RBFI) [16]:

$$\varphi^{(l)}_{t+\Delta t}(\boldsymbol{\xi})=\sum_{i=1}^{m}N(\boldsymbol{\xi}_i)\varphi^{(l)}_{t+\Delta t}(\boldsymbol{\xi}_i)=\mathbf{N}^{\mathrm{T}}(\boldsymbol{\xi})\boldsymbol{\varphi}^{(l)}_{t+\Delta t} \tag{10}$$

where m is the virtual node number within the current support domain of the $\boldsymbol{\xi}$ point, $\boldsymbol{\xi}_i$ the i^{th}

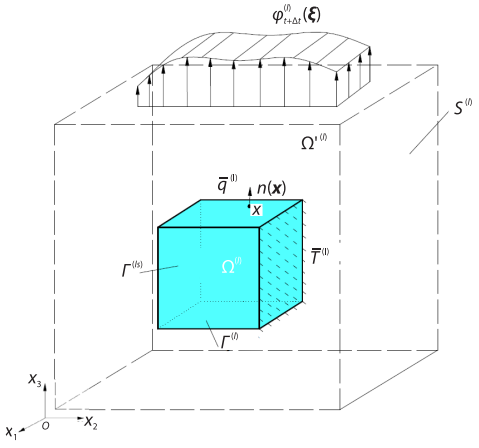

Figure 2. Schematic diagram of VBEM for any 3-D subdomain non-homogeneous media

virtual node, and $N(\boldsymbol{\xi}_i)$ – the shape function about the virtual node $\boldsymbol{\xi}_i$. Assume that there are $VN^{(l)}$ virtual nodes on the $S^{(l)}$ within the $\Omega^{(l)}$. The $\mathbf{N}^{\mathrm{T}}(\boldsymbol{\xi})$ and $\boldsymbol{\varphi}_{t+\Delta t}^{(l)}$ are the matrices of the shape functions and the virtual source functions:

$$\mathbf{N}^{\mathrm{T}}(\boldsymbol{\xi}) = \left\{ N(\boldsymbol{\xi}_1) \quad N(\boldsymbol{\xi}_2) \quad \cdots \quad N(\boldsymbol{\xi}_{VN^{(l)}}) \right\} \tag{11}$$

$$\boldsymbol{\varphi}_{t+\Delta t}^{(l)} = \left\{ \varphi_{t+\Delta t}^{(l)}(\boldsymbol{\xi}_1) \quad \varphi_{t+\Delta t}^{(l)}(\boldsymbol{\xi}_2) \quad \cdots \quad \varphi_{t+\Delta t}^{(l)}(\boldsymbol{\xi}_{VN^{(l)}}) \right\}^{\mathrm{T}} \tag{12}$$

Expressions of $T_{t+\Delta t}^{(l)hs}(\boldsymbol{x})$ and $q_{t+\Delta t}^{(l)hs}(\boldsymbol{x})$ by VBEM:

$$\begin{aligned} T_{t+\Delta t}^{(l)hs}(\boldsymbol{x}) &= \int_{S^{(l)}} T^*(\boldsymbol{x},\boldsymbol{\xi})\varphi_{t+\Delta t}^{(l)}(\boldsymbol{\xi})\mathrm{d}S = \\ &= \sum_{e'=1}^{m_{e'}} \sum_{g'=1}^{e_{e'}} \tilde{w}_1\left(\boldsymbol{\xi}_{g'}^{e'}\right)\tilde{w}_2\left(\boldsymbol{\xi}_{g'}^{e'}\right) J' T^*\left(\boldsymbol{x},\boldsymbol{\xi}_{g'}^{e'}\right)\varphi_{t+\Delta t}^{(l)}\left(\boldsymbol{\xi}_{g'}^{e'}\right) = \\ &= \sum_{e'=1}^{m_{e'}} \sum_{g'=1}^{e_{e'}} \tilde{w}_1\left(\boldsymbol{\xi}_{g'}^{e'}\right)\tilde{w}_2\left(\boldsymbol{\xi}_{g'}^{e'}\right) J' T^*\left(\boldsymbol{x},\boldsymbol{\xi}_{g'}^{e'}\right)\mathbf{N}^{\mathrm{T}}\left(\boldsymbol{\xi}_{g'}^{e'}\right)\tilde{\boldsymbol{\varphi}}_{t+\Delta t}^{(l)} \end{aligned} \tag{13}$$

$$\begin{aligned} q_{t+\Delta t}^{(l)hs}(\boldsymbol{x}) &= \int_{S^{(l)}} q^*(\boldsymbol{x},\boldsymbol{\xi})\varphi_{t+\Delta t}^{(l)}(\boldsymbol{\xi})\mathrm{d}S = \\ &= \sum_{e'=1}^{m_{e'}} \sum_{g'=1}^{e_{e'}} \tilde{w}_1\left(\boldsymbol{\xi}_{g'}^{e'}\right)\tilde{w}_2\left(\boldsymbol{\xi}_{g'}^{e'}\right) J' q^*\left(\boldsymbol{x},\boldsymbol{\xi}_{g'}^{e'}\right)\varphi_{t+\Delta t}^{(l)}\left(\boldsymbol{\xi}_{g'}^{e'}\right) = \\ &= \sum_{e'=1}^{m_{e'}} \sum_{g'=1}^{e_{e'}} \tilde{w}_1\left(\boldsymbol{\xi}_{g'}^{e'}\right)\tilde{w}_2\left(\boldsymbol{\xi}_{g'}^{e'}\right) J' q^*\left(\boldsymbol{x},\boldsymbol{\xi}_{g'}^{e'}\right)\mathbf{N}^{\mathrm{T}}\left(\boldsymbol{\xi}_{g'}^{e'}\right)\tilde{\boldsymbol{\varphi}}_{t+\Delta t}^{(l)} \end{aligned} \tag{14}$$

where $m_{e'}$ is the element number on the $S^{(l)}$, e' – the Gauss point number within virtual element, J' – the Jacobian of virtual element, $\xi_{g'}^{e'}$ – the q'^{th} Gauss point of the e'^{th} virtual element on the virtual boundary $S^{(l)}$, $\tilde{w}_1(\xi_{g'}^{e'})$ and $\tilde{w}_2(\xi_{g'}^{e'})$ are the weighting coefficients of the Gauss integral within the virtual element, $T^*(\boldsymbol{x}, \boldsymbol{\xi}_g^{e'})$ and $q^*(\boldsymbol{x}, \boldsymbol{\xi}_g^{e'})$ are the fundamental solutions of temperature and thermal flux for 3-D thermal analysis. The $T^*(\boldsymbol{x}, \boldsymbol{\xi}_g^{e'}) = 1/4\pi r$, $q^*(\boldsymbol{x}, \boldsymbol{\xi}_g^{e'}) = -k^{(l)}\partial T^*(\boldsymbol{x}, \boldsymbol{\xi}_g^{e'})/\partial n$, where r is the distance between $\boldsymbol{x}$ and $\boldsymbol{\xi}_g^{e'}$:

Special solutions

The $T_{t+\Delta t}^{(l)ss}(\boldsymbol{x})$ and $q_{t+\Delta t}^{(l)ss}(\boldsymbol{x})$ are gotten by RBFI within the l^{th} subdomain $\Omega^{(l)}$.

The $T_{t+\Delta t}^{(l)ss}(\boldsymbol{x})$ is shown [16]:

$$T_{t+\Delta t}^{(l)ss}(\boldsymbol{x}) = \sum_{k=1}^{DN^{(l)}} f_{t+\Delta t}^{(l)}(\boldsymbol{x},\boldsymbol{x}_k)\beta_{t+\Delta t}^{(l)}(\boldsymbol{x}_k) \tag{15}$$

where $DN(l)$ is the virtual node number within the subdomain $\Omega^{(l)}$, $\beta_{t+\Delta t}^{(l)}(\boldsymbol{x}_k)$ – the coefficient to be solved, $f_{t+\Delta t}^{(l)}(\boldsymbol{x}, \boldsymbol{x}_k) = r^2/6 + r^5/30$, where r is the distance between $\boldsymbol{x}$ and $\boldsymbol{x}_k$:

The $q_{t+\Delta t}^{(l)ss}(\boldsymbol{x})$ is:

$$q_{t+\Delta t}^{(l)ss}(\boldsymbol{x}) = \sum_{k=1}^{DN^{(l)}} -k^{(l)} \frac{\partial f_{t+\Delta t}^{(l)}(\boldsymbol{x},\boldsymbol{x}_k)}{\partial n} \beta_{t+\Delta t}^{(l)}(\boldsymbol{x}_k) \tag{16}$$

Unified forms of solutions

Submitting eqs. (13)-(16) into eqs. (8) and (9), eqs. (8) and (9) can be re-written and expanded to all unknowable coefficients:

$$\begin{aligned} T_{t+\Delta t}^{(l)}(\boldsymbol{x}) &= \sum_{e'=1}^{m_{e'}}\sum_{g'=1}^{e_{e'}} \tilde{w}_1\left(\boldsymbol{\xi}_{g'}^{e'}\right)\tilde{w}_2\left(\boldsymbol{\xi}_{g'}^{e'}\right) J'T^*\left(\boldsymbol{x},\boldsymbol{\xi}_{g'}^{e'}\right)\mathbf{N}^{\mathrm{T}}\left(\boldsymbol{\xi}_{g'}^{e'}\right)\tilde{\boldsymbol{\varphi}}_{t+\Delta t}^{(l)} + \\ &+ \sum_{k=1}^{DN(l)} f_{t+\Delta t}^{(l)k}(\boldsymbol{x},\boldsymbol{x}_k)\beta_{t+\Delta t}^{(l)}(\boldsymbol{x}_k) \\ &= \mathbf{U}_{t+\Delta t}\boldsymbol{\Psi}_{t+\Delta t} \end{aligned} \tag{17}$$

$$\begin{aligned} q_{t+\Delta t}^{(l)}(\boldsymbol{x}) &= \sum_{e'=1}^{m_{e'}}\sum_{g'=1}^{e_{e'}} \tilde{w}_1\left(\boldsymbol{\xi}_{g'}^{e'}\right)\tilde{w}_2\left(\boldsymbol{\xi}_{g'}^{e'}\right) J'q^*\left(\boldsymbol{x},\boldsymbol{\xi}_{g'}^{e'}\right)\mathbf{N}^{\mathrm{T}}\left(\boldsymbol{\xi}_{g'}^{e'}\right)\tilde{\boldsymbol{\varphi}}_{t+\Delta t}^{(l)} + \\ &+ \sum_{k=1}^{DN(l)} -k(l)\frac{\partial f_{t+\Delta t}^{(l)k}(\boldsymbol{x},\boldsymbol{x}_k)}{\partial n}\beta_{t+\Delta t}^{(l)}(\boldsymbol{x}_k) \\ &= \mathbf{P}_{t+\Delta t}\boldsymbol{\Psi}_{t+\Delta t} \end{aligned} \tag{18}$$

where the matrices $\boldsymbol{\Psi}_{t+\Delta t}$, $\mathbf{U}_{t+\Delta t}$, and $\mathbf{P}_{t+\Delta t}$ are expressed as:

$$\begin{aligned} \boldsymbol{\Psi}_{t+\Delta t} &= \Big\{\varphi_{t+\Delta t}^{(1)}(\boldsymbol{\xi}_1),\cdots,\varphi_{t+\Delta t}^{(1)}(\boldsymbol{\xi}_{VN^{(1)}}),\beta_{t+\Delta t}^{(1)}(\boldsymbol{x}_1),\cdots,\beta_{t+\Delta t}^{(1)}(\boldsymbol{x}_{DN^{(1)}}), \\ &\cdots,\varphi_{t+\Delta t}^{(l)}(\boldsymbol{\xi}_1),\cdots,\varphi_{t+\Delta t}^{(l)}(\boldsymbol{\xi}_{VN^{(l)}}),\beta_{t+\Delta t}^{(l)}(\boldsymbol{x}_1),\cdots,\beta_{t+\Delta t}^{(l)}(\boldsymbol{x}_{DN^{(l)}}), \\ &\cdots,\varphi_{t+\Delta t}^{(n)}(\boldsymbol{\xi}_1),\cdots,\varphi_{t+\Delta t}^{(n)}(\boldsymbol{\xi}_{VN^{(n)}}),\beta_{t+\Delta t}^{(n)}(\boldsymbol{x}_1),\cdots,\beta_{t+\Delta t}^{(n)}(\boldsymbol{x}_{DN^{(n)}})\Big\}^T \\ &= \left\{\Psi_{t+\Delta t}^{1},\ \cdots,\ \Psi_{t+\Delta t}^{I},\ \cdots,\ \Psi_{t+\Delta t}^{NT}\right\}^T \end{aligned} \tag{19}$$

$$\mathbf{U}_{t+\Delta t} = \left\{U_{t+\Delta t}^{1},\ \cdots,\ U_{t+\Delta t}^{I},\ \cdots,\ U_{t+\Delta t}^{NT}\right\} \tag{20}$$

$$\mathbf{P}_{t+\Delta t} = \left\{P_{t+\Delta t}^{1},\ \cdots,\ P_{t+\Delta t}^{I},\ \cdots,\ P_{t+\Delta t}^{NT}\right\} \tag{21}$$

where NT is the total number of unknowable coefficients, namely $NT = \sum_{l=1}^{n}(VN^{(l)} + DN^{(l)})$, $U_{t+\Delta t}^{I}$ and $P_{t+\Delta t}^{I}$ are the term of integral accumulations of the virtual source functions or the term of the unknowable coefficient within the l^{th} subdomain $\Omega^{(l)}$, and are written:

$$U_{t+\Delta t}^{I} = \sum_{k=1}^{K}\tilde{w}_1\left(\boldsymbol{\xi}_{g'}^{e'}\right)\tilde{w}_2\left(\boldsymbol{\xi}_{g'}^{e'}\right)J'T^*\left(\boldsymbol{x},\boldsymbol{\xi}_{g'}^{e'}\right)N\left(\boldsymbol{\xi}_{g'}^{e'}\right)\ \text{or}\ f_{t+\Delta t}^{I}\left(\boldsymbol{x},\boldsymbol{x}_k\right) \tag{22}$$

$$P_{t+\Delta t}^{I} = \sum_{k=1}^{K}\tilde{w}\left(\boldsymbol{\xi}_{g'}^{e'}\right)J'q^*\left(\boldsymbol{x},\boldsymbol{\xi}_{g'}^{e'}\right)N\left(\boldsymbol{\xi}_{g'}^{e'}\right)\ \text{or}\ -k^{(l)}(\boldsymbol{x})\frac{\partial f_{t+\Delta t}(\boldsymbol{x},\boldsymbol{x}_k)}{\partial n} \tag{23}$$

where K is the Gauss point number in the current support domain of the node I on the boundary $S^{(l)}$.

Similarly, submitting eqs. (17) and (18) into eq. (2), eq. (2) can be re-expressed:

$$
\begin{aligned}
&\rho^{(l)}c^{(l)}T_t^{(l)}(\boldsymbol{x})/\Delta t+Q_{t+\Delta t}^{(l)}(\boldsymbol{x})=\\
&=\rho^{(l)}c^{(l)}T_{t+\Delta t}^{(l)}(\boldsymbol{x})/\Delta t-k^{(l)}(\boldsymbol{x})\nabla^2T_{t+\Delta t}^{(l)}(\boldsymbol{x})-\nabla k^{(l)}(\boldsymbol{x})\nabla T_{t+\Delta t}^{(l)}(\boldsymbol{x})=\\
&\quad=\sum_{e'=1}^{m_{e'}}\sum_{g'=1}^{e_{e'}}\tilde{w}_1\left(\boldsymbol{\xi}_{g'}^{e'}\right)\tilde{w}_2\left(\boldsymbol{\xi}_{g'}^{e'}\right)J'\begin{bmatrix}\rho^{(l)}c^{(l)}T^*(\boldsymbol{x},\boldsymbol{\xi}_{g'}^{e'})/\Delta t\\-k^{(l)}(\boldsymbol{x})\nabla^2T^*(\boldsymbol{x},\boldsymbol{\xi}_{g'}^{e'})\\-\nabla k^{(l)}(\boldsymbol{x})\nabla T^*(\boldsymbol{x},\boldsymbol{\xi}_{g'}^{e'})\end{bmatrix}\mathbf{N}^{\mathrm{T}}\left(\boldsymbol{\xi}_{g'}^{e'}\right)\tilde{\boldsymbol{\varphi}}_{t+\Delta t}^{(l)}\\
&\quad+\sum_{}^{DN^{(l)}}\begin{bmatrix}\rho^{(l)}c^{(l)}f_{t+\Delta t}^{(l)}(\boldsymbol{x},\boldsymbol{x}_k)/\Delta t\\-k^{(l)}(\boldsymbol{x})\nabla^2f_{t+\Delta t}^{(l)}(\boldsymbol{x},\boldsymbol{x}_k)\\-\nabla k^{(l)}(\boldsymbol{x})\nabla f_{t+\Delta t}^{(l)}(\boldsymbol{x},\boldsymbol{x}_k)\end{bmatrix}\beta_{t+\Delta t}^{(l)k}(\boldsymbol{x}_k)\\
&\quad=\mathbf{Q}_{t+\Delta t}\boldsymbol{\Psi}_{t+\Delta t}\\
&\quad=\left\{Q_{t+\Delta t}^1,\cdots,Q_{t+\Delta t}^I,\cdots,Q_{t+\Delta t}^{NT}\right\}\left\{\Psi_{t+\Delta t}^1,\cdots,\Psi_{t+\Delta t}^I,\cdots,\Psi_{t+\Delta t}^{NT}\right\}^{\mathrm{T}}
\end{aligned}
\tag{24}
$$

here $Q_{t+\Delta t}^I$ is also the integral term accumulations or the term of the unknowable coefficient about the node I within the l^{th} subdomain $\Omega(l)$:

$$
Q_{t+\Delta t}^I=\sum_{k=1}^{K}\tilde{w}_1\left(\boldsymbol{\xi}_{g'}^{e'}\right)\tilde{w}_2\left(\boldsymbol{\xi}_{g'}^{e'}\right)J'\begin{bmatrix}\dfrac{\rho^{(l)}c^{(l)}T^*\left(\boldsymbol{x},\boldsymbol{\xi}_{g'}^{e'}\right)}{\Delta t}\\-k^{(l)}(\boldsymbol{x})\nabla^2T^*\left(\boldsymbol{x},\boldsymbol{\xi}_{g'}^{e'}\right)\\-\nabla k^{(l)}(\boldsymbol{x})\nabla T^*\left(\boldsymbol{x},\boldsymbol{\xi}_{g'}^{e'}\right)\end{bmatrix}N\left(\boldsymbol{\xi}_{g'}^{k}\right)\text{ or }\begin{bmatrix}\dfrac{\rho^{(l)}c^{(l)}f_{t+\Delta t}^{(l)}(\boldsymbol{x},\boldsymbol{x}_k)}{\Delta t}\\-k^{(l)}(\boldsymbol{x})\nabla^2f_{t+\Delta t}^{(l)}(\boldsymbol{x},\boldsymbol{x}_k)\\-\nabla k^{(l)}(\boldsymbol{x})\nabla f_{t+\Delta t}^{(l)}(\boldsymbol{x},\boldsymbol{x}_k)\end{bmatrix}=0 \tag{25}
$$

Calculation scheme

Considering the control eq. (2), the boundary and continuous conditions eqs. (3)-(7), and using the Galerkin method, assuming $Q_{t+\Delta t}^{(l)}$ as the known internal thermal source, the integral formula of VBMGM for 3-D multi-domain transient thermal analysis with variable thermal sources in non-homogeneous media can be obtained:

$$
\sum_{l=1}^{n}\left\{\begin{aligned}
&w_1\int_{x\in\Gamma_T^{(l)}}\left[T_{t+\Delta t}^{(l)}(\boldsymbol{x})-\overline{T}_{t+\Delta t}^{(l)}(\boldsymbol{x})\right]\mathrm{d}\Gamma(\boldsymbol{x})\\
&+w_2\int_{x\in\Gamma_q^{(l)}}\left[q_{t+\Delta t}^{(l)}(\boldsymbol{x})-\overline{q}_{t+\Delta t}^{(l)}(\boldsymbol{x})\right]\mathrm{d}\Gamma(\boldsymbol{x})\\
&+w_3\int_{x\in\Omega_I^{(l)}}\left[Q_{t+\Delta t}^{(l)}(\boldsymbol{x})-\overline{Q}_{t+\Delta t}^{(l)}(\boldsymbol{x})\right]\mathrm{d}\Omega(\boldsymbol{x})
\end{aligned}\right\}+\sum_{G=ls}\left\{\begin{aligned}
&w_4\int_{x\in\Gamma^{(ls)}}\left[T_{t+\Delta t}^{(l)}(\boldsymbol{x})-T_{t+\Delta t}^{(s)}(\boldsymbol{x})\right]\mathrm{d}\Gamma(\boldsymbol{x})\\
&+w_5\int_{x\in\Gamma^{(ls)}}\left[q_{t+\Delta t}^{(l)}(\boldsymbol{x})-q_{t+\Delta t}^{(s)}(\boldsymbol{x})\right]\mathrm{d}\Gamma(\boldsymbol{x})
\end{aligned}\right\}=0 \tag{26}
$$

where the weighting coefficients $w_1 = \delta[T_{t+\Delta t}^{(l)}(\boldsymbol{x})]$, $w_2 = \delta[q_{t+\Delta t}^{(l)}(\boldsymbol{x})]$, $w_3 = \delta[q_{t+\Delta t}^{(l)}(\boldsymbol{x})]$, $w_4 = \delta[T_{t+\Delta t}^{(l)}(\boldsymbol{x}) - T_{t+\Delta t}^{(s)}(\boldsymbol{x})]$, and $w_5 = \delta[q_{t+\Delta t}^{(l)}(\boldsymbol{x}) + q_{t+\Delta t}^{(s)}(\boldsymbol{x})]$, and δ is the variational symbol.

In due to $\partial T_{t+\Delta t}^{(l)}(\boldsymbol{x})/\partial\Psi_{t+\Delta t}^I = U_{t+\Delta t}^I$ and $\partial Q_{t+\Delta t}^{(l)}(\boldsymbol{x})/\partial\Psi_{t+\Delta t}^I = Q_{t+\Delta t}^I$, submitting eqs. (17), (18), and (24) into eq. (26), the discrete formula of VBMGM for 3-D multi-domain transient thermal analysis with variable thermal sources in non-homogeneous media can be re-written into matrix form:

$$\mathbf{C}_{t+\Delta t} = \mathbf{\Psi}_{t+\Delta t} = \mathbf{D}_{t+\Delta t} \tag{27}$$

where the coefficient matrix $\mathbf{C}_{t+\Delta t} = [C^{mn}_{t+\Delta t}]_{NT\times NT}$ is sparse and symmetric, the right-hand known matrix $\mathbf{D}_{t+\Delta t} = [D^{mn}_{t+\Delta t}]_{NT\times 1}$ based on the real and continuous boundary conditions and thermal sources in each subdomain. The expressions of $C^{mn}_{t+\Delta t}$ and $D^{mn}_{t+\Delta t}$ are obtained:

$$\begin{aligned} C^{mn}_{t+\Delta t}(\boldsymbol{x}) = &\sum_{l=1}^{n}\left\{U^m_{t+\Delta t}U^n_{t+\Delta t} + P^m_{t+\Delta t}P^n_{t+\Delta t} + Q^m_{t+\Delta t}Q^n_{t+\Delta t}\right\} + \\ &+ \sum_{G(\Gamma ls)}\left(U^m_{t+\Delta t} - U^m_{t+\Delta t}\right)\left(U^n_{t+\Delta t} - U^n_{t+\Delta t}\right) + \left(P^m_{t+\Delta t} + P^m_{t+\Delta t}\right)\left(P^n_{t+\Delta t} + P^n_{t+\Delta t}\right) \end{aligned} \tag{28}$$

$$D^m_{t+\Delta t} = \sum_{l=1`}^{n} U^m_{t+\Delta t}\bar{T}^{(l)}_{t+\Delta t}(\boldsymbol{x}) + P^m_{t+\Delta t}\bar{q}^{(l)}_{t+\Delta t}(\boldsymbol{x}) + Q^m_{t+\Delta t}\left[\bar{Q}_{t+\Delta t}(\boldsymbol{x}) + \rho c\frac{T_t(\boldsymbol{x})}{\Delta t}\right] \tag{29}$$

It can be found that $w_1 = U^m_{t+\Delta t}$, $w_2 = P^m_{t+\Delta t}$, $w_3 = Q^m_{t+\Delta t}$, $w_4 = U^m_{t+\Delta t} - U^m_{t+\Delta t}$, and $w_5 = P^m_{t+\Delta t} + P^m_{t+\Delta t}$ of eq. (26).

Implementation process

It is assumed that the time of computation for transient thermal conduction problems is recorded as $t_{\text{calculation}} \times t_{\text{calculation}}$ can be divided into n parts. Each part is Δt. Therefore, $t_{\text{calculation}} = [t_0, t_0 + \Delta t, t_1 + \Delta t, \ldots, t_{n-1} + \Delta t]$. Since the boundary conditions at t_0 are known, the unknowable $\mathbf{\Psi}_{t_0+\Delta t}$ can be obtained by eq. (27). Submitting $\mathbf{\Psi}_{t_0+\Delta t}$ into eqs. (17), (18), and (24), $T^{(l)}_{t_0+\Delta t}(\boldsymbol{x})$, $q^{(l)}_{t_0+\Delta t}(\boldsymbol{x})$, and $Q^{(l)}_{t_0+\Delta t}(\boldsymbol{x})$ can be computed. Importing $T^{(l)}_{t_0+\Delta t}(\boldsymbol{x})$, $q^{(l)}_{t_0+\Delta t}(\boldsymbol{x})$, and $Q^{(l)}_{t_0+\Delta t}(\boldsymbol{x})$ into eq. (27), $\mathbf{\Psi}_{t_1+\Delta t}$ can be gotten. The $\mathbf{\Psi}_{t_{n-1}+\Delta t}$, $T^{(l)}_{t_{n-1}+\Delta t}(\boldsymbol{x})$, $q^{(l)}_{t_{n-1}+\Delta t}(\boldsymbol{x})$, and $Q^{(l)}_{t_{n-1}+\Delta t}(\boldsymbol{x})$ namely $\mathbf{\Psi}_{t\text{calculation}}$, $T^{(l)}_{t\text{calculation}}(\boldsymbol{x})$, $q^{(l)}_{t\text{calculation}}(\boldsymbol{x})$, and $Q^{(l)}_{t\text{calculation}}(\boldsymbol{x})$ are finally obtained by solving in turn.

Numerical examples

Example 1. The cube with variable thermal conductivity and thermal sources.

The cube with variable thermal conductivity thermal sources (region [1, 1, 1] m × [2, 2, 2] m according to [x, y, z] co-ordinates) is shown in fig. 3. The surrounding boundary conditions are $T(\boldsymbol{x}, t) = x^2 + y^2 + z^2 + \sin(10t)$ [°C]. Thermal conductivity $k(\boldsymbol{x}) = \boldsymbol{x} + y + z$ [W/m°C]. Density $\rho = 1$ kg/m^3. Specific thermal capacity $c = 1$ J/(kg°C). Thermal source $Q(\boldsymbol{x}, t) = -8(\boldsymbol{x} + y + z) + 10\cos(10t)$ [W/m^3]. The starting temperature changed $T(\boldsymbol{x}, 0) = \boldsymbol{x}^2 + y^2 + z^2$ [°C].

It should be noted that the divisions of elements and extraction of nodes of this paper are obtained by Mesh200 element of ANSYS software. The prepossessing data are imported into our own program, and then the numerical results are calculated. The discretization of the real boundaries is exhibited in fig. 4. Each face of real boundaries is divided into 16 elements. The virtual boundary is 0.1 m away from the real boundary. Each face of virtual boundaries is also divided into 16 elements. The nodes for interpolation of thermal sources are obtained by dividing the cube using Solid65 elements of ANSYS software, as shown in fig. 5. There are 125 nodes in fig. 5. The number of virtual elements and virtual nodes is identical. Virtual nodes are positioned at the midpoint of their virtual elements. The construction of the virtual source function utilizes 8 virtual nodes. Each virtual or real element adopts 4 Gauss points for integration. The exact solutions $T(x, t) = \boldsymbol{x}^2 + y^2 + z^2 + \sin(10t)$ [°C] [17-19]. The radial integration boundary-element method with finite difference (RIBEM-FD) [17] and the precise time-domain boundary-element method (PTBEM) [18] were also used to calculate this problem. The Δt of two numerical methods were 0.0001 second and 0.001 second, respectively. For comparison,

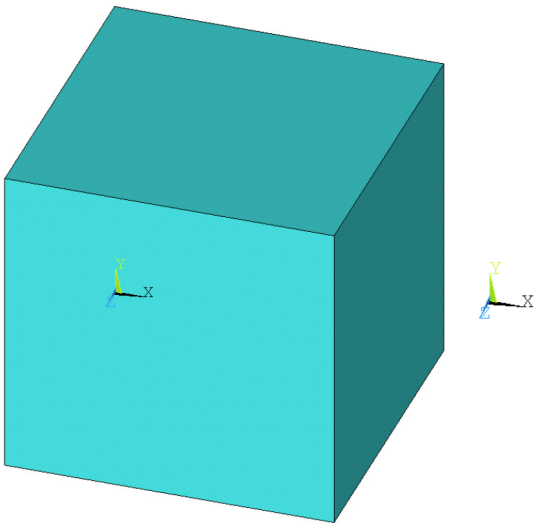

Figure 3. The calculation model of the cube with variable thermal conductivity and thermal sources

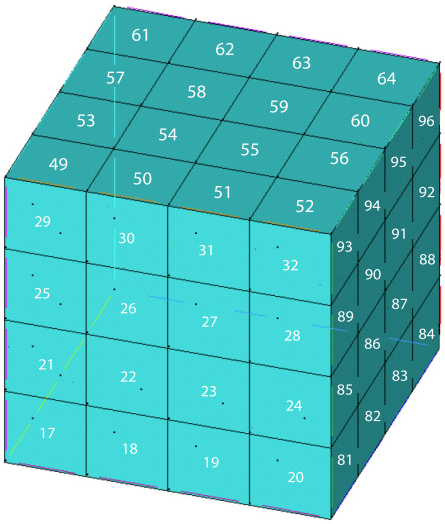

Figure 4. Schematic diagram of real boundaries for the cube with variable thermal conductivity and thermal sources

Δt is taken as 0.0001second in the paper. The corresponding results are shown in fig. 6. The RMSE is the root mean square error defined as [17]:

$$RMSE = \sqrt{\frac{\sum_{i=1}^{N}\left(T^i_{\text{numerical}} - T^i_{\text{exact}}\right)^2}{\sum_{i=1}^{N}\left(T^i_{\text{exact}}\right)^2}}$$

where $T^i_{\text{numerical}}$ and T^i_{exact} are the numerical result and exact solution of the i^{th} real node and N – the number of the real nodes. We can see that RMSE of this paper is smaller than the other two at 1-3 seconds and slightly larger at the latter two seconds.

Take $\Delta t = 0.1$ second and calculate the temperatures at different times when $z = 1.5$ m, namely half of the cube along the z-axis in tab. 1. In tab. 2, the distance between the virtual and real boundaries has been altered to reveal the exactness of this method. The stability and exactness of the proposed method can be observed from tab. 1 and tab. 2.

Example 2. The cuboid of three subdomains with variable boundary conditions and starting temperature (the first subdomain [1, 1, 1] m × [2, 2, 2] m, the second subdomain [1, 1, 2] m × [2, 2, 3] m and the third subdomain [1, 1, 3] m × [2, 2, 4] m according to [x, y, z] co-ordinates) is given in fig. 7. The surrounding boundary conditions of the cuboid with three subdomains are $T(\boldsymbol{x}, t) = [\sin(\pi, \boldsymbol{x}) + \sin(\pi, y) + \sin(\pi, z)]e^{-k\pi^2 t}$ [°C]. The continuous boundary conditions between subdomains should be considered here. Thermal conductivity $k_1(x) = k_2(x) = k_3(x) = 0.1$ W/m°C. Density $\rho_1 = \rho_2 = \rho_3 = 1$ kg/m^3. Specific thermal capacity $c_1 = c_2 = c_3 = 1$ J/kg°C. Thermal source $Q_1(\boldsymbol{x}, t) = Q_2(\boldsymbol{x}, t) = Q_3(\boldsymbol{x}, t) = 0$. The starting temperature changed is $T(\boldsymbol{x}, 0) = \sin(\pi \boldsymbol{x}) + \sin(\pi y) + \sin(\pi z)$.

Because discretizations of the three subdomains are similar, only the schematic diagram of the first subdomain (spherical surface with radius 1m, the spherical center co-ordinates $\boldsymbol{x} = 1.5$ m, $y = 1.5$ m, $z = 1.5$ m) is given to illustrate the stability of this method, as shown in fig. 7. There are 88 virtual boundary elements in fig. 8. There is no need to interpolate the thermal

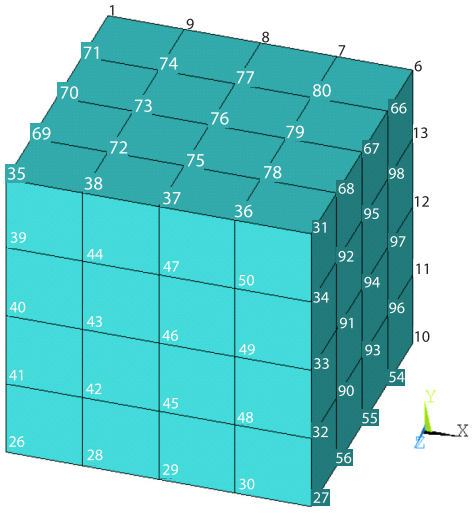

Figure 5. Schematic diagram of thermal source interpolation for the cube with variable thermal conductivity thermal sources

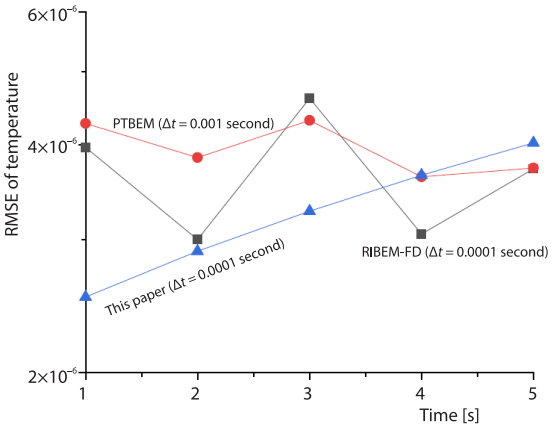

Figure 6. The RMES of temperature for *Example 1*

Table 1. Temperatures of the cube with variable thermal conductivity thermal sources

Co-ordinates			t = 0.2 second		t = 0.5 second		t = 1 second	
x	y	z	Paper	Exact solution	Paper	Exact solution	Paper	Exact solution
1.00	1.00	1.50	5.1387	5.1593	3.2779	3.2911	3.6902	3.7060
2.00	1.00	1.50	8.1115	8.1593	6.2517	6.2911	6.6636	6.7060
1.33	1.00	1.50	5.9402	5.9371	4.0899	4.0689	4.5001	4.4838
1.67	1.00	1.50	6.9404	6.9371	5.0900	5.0689	5.5002	5.4838
2.00	2.00	1.50	11.0128	11.1593	9.1573	9.2911	9.5694	9.7060
2.00	1.33	1.50	8.8503	8.9371	6.9993	7.0689	7.4098	7.4838
2.00	1.67	1.50	9.8222	9.9371	7.9726	8.0689	8.3832	8.4838
1.00	2.00	1.50	8.1156	8.1593	6.2554	6.2911	6.6674	6.7060
1.67	2.00	1.50	9.8236	9.9371	7.9739	8.0689	8.3845	8.4838
1.33	2.00	1.50	8.8537	8.9371	7.0024	7.0689	7.4130	7.4838
1.00	1.67	1.50	6.9409	6.9371	5.0904	5.0689	5.5006	5.4838
1.00	1.33	1.50	5.9393	5.9371	4.0891	4.0689	4.4993	4.4838
1.33	1.33	1.50	6.8403	6.7149	4.9621	4.8466	5.4561	5.2615
1.33	1.67	1.50	7.8242	7.7149	5.9389	5.8466	6.4347	6.2615
1.67	1.33	1.50	7.8232	7.7149	5.9380	5.8466	6.4339	6.2615
1.67	1.67	1.50	8.8042	8.7149	6.9135	6.8466	7.4108	7.2615

source in this example. The discrete process of real boundaries of the first subdomain is similar to *Example 1*. The virtual or real boundaries of other subdomains are similar to the first subdomain. Each virtual or real element adopts 4 Gauss points for integration. The exact solution of the example is $T(\boldsymbol{x}, t) = [\sin(\pi x) + \sin(\pi y) + \sin(\pi z)]e^{-\pi 2t}$ [°C] [19]. Taking $\Delta t = 0.1$ second. The

Table 2. Temperatures of the cube with variable thermal conductivity thermal sources, when changing the distance between the virtual boundary and the real boundary

Co-ordinates			Exact solution	The distance between virtual and real boundaries				
x	*y*	*z*		0.01 m	0.15 m	0.2 m	0.5 m	1.0 m
1.00	1.00	1.50	3.7060	3.9783	3.7150	3.7139	3.7069	3.7089
2.00	1.00	1.50	6.7060	6.7192	6.6831	6.6927	6.7062	6.7054
1.33	1.00	1.50	4.4838	4.8114	4.5007	4.4928	4.4840	4.4841
1.67	1.00	1.50	5.4838	5.7626	5.4926	5.4872	5.4839	5.4839
2.00	2.00	1.50	9.7060	9.5301	9.6544	9.6811	9.7058	9.7088
2.00	1.33	1.50	7.4838	7.4782	7.4470	7.4673	7.4836	7.4838
2.00	1.67	1.50	8.4838	8.4524	8.4395	8.4656	8.4835	8.4839
1.00	2.00	1.50	6.7060	6.7291	6.6836	6.6929	6.7061	6.7065
1.67	2.00	1.50	8.4838	8.4649	8.4396	8.4656	8.4835	8.4841
1.33	2.00	1.50	7.4838	7.4934	7.4475	7.4674	7.4836	7.4838
1.00	1.67	1.50	5.4838	5.7645	5.4926	5.4872	5.4839	5.4839
1.00	1.33	1.50	4.4838	4.8111	4.5005	4.4927	4.4840	4.4837
1.33	1.33	1.50	5.2615	5.6338	5.4656	5.4675	5.4681	5.4682
1.33	1.67	1.50	6.2615	6.5493	6.4518	6.4568	6.4583	6.4582
1.67	1.33	1.50	6.2615	6.5440	6.4516	6.4569	6.4585	6.4585
1.67	1.67	1.50	7.2615	7.4703	7.4394	7.4480	7.4506	7.4506

Example 2. The cuboid of three subdomains with variable boundary conditions and starting temperature.

results of the calculations are presented in half of the second cube along the *z*-axis in tab. 3. The proposed method's stability and exactness are validated.

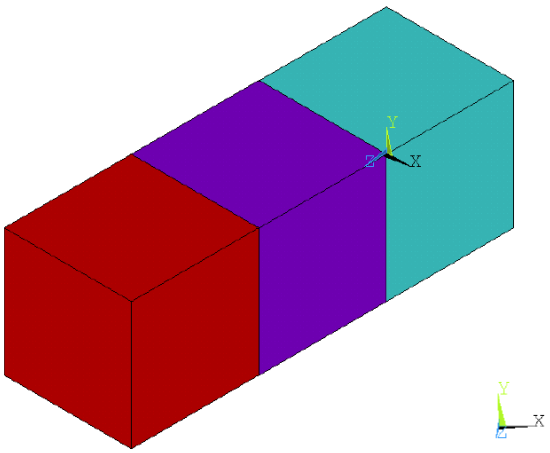

Figure 7. The calculation model of the cuboid of three subdomains with variable boundary conditions and starting temperature

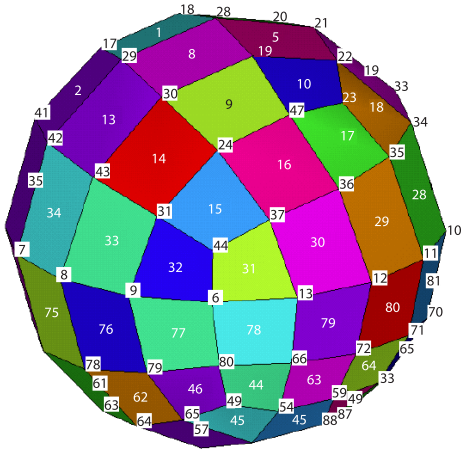

Figure 8. Schematic diagram of virtual boundaries for only the first subdomain of *Example 2*

Table 3. Temperatures of the cuboid of three subdomains with variable boundary conditions and starting temperature

Co-ordinates			t = 0.1 second		t = 0.4 second		t = 0.8 second		t = 5 seconds	
x	y	z	Paper	Exact solution	Paper	Exact solution	Paper	Exact solution	Paper	Exact solution
1	1	1.5	–0.9050	–0.9060	–0.6731	–0.6738	–0.4535	–0.4540	–0.0072	–0.0072
2	1	1.5	–0.9082	–0.9060	–0.6755	–0.6738	–0.4551	–0.4540	–0.0072	–0.0072
1.25	1	1.5	–1.5423	–1.5467	–1.1470	–1.1503	–0.7729	–0.7751	–0.0122	–0.0123
1.5	1	1.5	–1.8138	–1.8120	–1.3489	–1.3477	–0.9089	–0.9081	–0.0144	–0.0144
1.75	1	1.5	–1.5476	–1.5467	–1.1510	–1.1503	–0.7756	–0.7751	–0.0123	–0.0123
2	2	1.5	–0.9040	–0.9060	–0.6723	–0.6738	–0.4530	–0.4540	–0.0072	–0.0072
2	1.25	1.5	–1.5507	–1.5467	–1.1533	–1.1503	–0.7771	–0.7751	–0.0123	–0.0123
2	1.5	1.5	–1.8074	–1.8120	–1.3442	–1.3477	–0.9057	–0.9081	–0.0143	–0.0144
2	1.75	1.5	–1.5509	–1.5467	–1.1535	–1.1503	–0.7772	–0.7751	–0.0123	–0.0123
1	2	1.5	–0.9058	–0.9060	–0.6737	–0.6738	–0.4539	–0.4540	–0.0072	–0.0072
1.75	2	1.5	–1.5482	–1.5467	–1.1514	–1.1503	–0.7758	–0.7751	–0.0123	–0.0123
1.5	2	1.5	–1.8111	–1.8120	–1.3470	–1.3477	–0.9076	–0.9081	–0.0144	–0.0144
1.25	2	1.5	–1.5469	–1.5467	–1.1505	–1.1503	–0.7752	–0.7751	–0.0123	–0.0123
1	1.75	1.5	–1.5478	–1.5467	–1.1512	–1.1503	–0.7757	–0.7751	–0.0123	–0.0123
1	1.5	1.5	–1.8074	–1.8120	–1.3442	–1.3477	–0.9058	–0.9081	–0.0143	–0.0144
1	1.25	1.5	–1.5517	–1.5467	–1.1540	–1.1503	–0.7776	–0.7751	–0.0123	–0.0123
1.25	1.25	1.5	–2.1966	–2.1873	–1.6164	–1.6268	–1.0849	–1.0962	–0.0178	–0.0174
1.25	1.5	1.5	–2.4580	–2.4527	–1.8323	–1.8241	–1.2256	–1.2291	–0.0190	–0.0195
1.25	1.75	1.5	–2.1967	–2.1873	–1.6164	–1.6268	-1.0849	–1.0962	–0.0178	–0.0174
1.5	1.25	1.5	–2.4583	–2.4527	–1.8325	–1.8241	-1.2396	–1.2291	–0.0190	–0.0195
1.5	1.5	1.5	–2.7009	–2.7181	–2.0380	–2.0215	-1.3670	–1.3621	–0.0216	–0.0216
1.5	1.75	1.5	–2.4581	–2.4527	–1.8323	–1.8241	–1.2256	–1.2291	–0.0190	–0.0195
1.75	1.25	1.5	–2.1967	–2.1873	–1.6164	–1.6268	–1.0849	–1.0962	–0.0178	–0.0174
1.75	1.5	1.5	–2.4680	–2.4527	–1.8323	–1.8241	–1.2256	–1.2291	–0.0190	–0.0195
1.75	1.75	1.5	–2.1867	–2.1873	–1.6165	–1.6268	–1.0849	–1.0962	–0.0178	–0.0174

Conclusions

An efficient boundary meshfree computational approach, namely VBMGM, for 3-D multi-domain transient thermal analysis with variable thermal sources in non-homogeneous media is presented. The examples of the cube with variable thermal conductivity and thermal sources and the cuboid of three subdomains with variable boundary conditions and starting temperature, are calculated. The proposed method's stability and exactness are validated.

The virtual source functions of the homogeneous solutions and the unknowable coefficients of the special solutions are constructed by RBFI. Unified forms of solutions of the temperature, the thermal flux, and the thermal source are obtained. Taking into account the Galerkin approach, the control equation, the boundary conditions, and continuous conditions, it is obtained that the detailed discrete formula of VBMGM for 3-D multi-domain transient ther-

mal analysis with variable thermal sources in non-homogeneous media. The coefficient matrix of its integral equation is sparse and symmetric.

The VBMGM has the benefits of BEM, meshfree method, and Galerkin method for 3-D multi-domain transient thermal analysis with variable thermal sources in non-homogeneous media. Its implementation process is shown. The proposed method is easily programmed and extended to deal with other 3-D multi-domain complex transient thermal conduction problems.

Acknowledgment

This work was supported by the National Natural Science Foundation of China (No. 11762005), Guizhou Province Science and Technology Plan Project (Qianke He Foundation-ZK [2021] Key 021).

Nomenclature

c – specific thermal capacity, [Jkg^{-1}°C^{-1}]
f – known interpolation function
k – thermal conductivity coefficient, [Wm^{-1}°C^{-1}]
Q – thermal source, [Wm^{-3}]
q – thermal flux, [Wm^{-2}]
r – the distance, [m]
S – virtual boundary
T – temperature, [°C]
w – weighting coefficient
$\boldsymbol{x}$ – point of real boundary

Greek symbols

β – unknown coefficient
δ – variational symbol
Γ – real boundary
$\boldsymbol{\xi}$ – point of virtual boundary
ρ – density, [kgm^{-3}]
φ – virtual source function
Ω – calculation domain

Topscripts

– – known value

Superscripts

(e') – the e'^{th}
hs – homogeneous solution
(l) – the l$^{\text{th}}$ virtual sub-domain
(s) – the s$^{\text{th}}$ virtual sub-domain
ss – special solution
$'$ – virtual domain
* – fundamental solution

Subscripts

t – t moment
Δt – time step, [second]
t_0 – initial moment
g' – the g'^{th}
1 – the first

References

[1] Jacinto, C. C., *et al.*, A New Approach for Solving Heat Conduction under Zero and Non-Zero Initial Conditions, *Engineering Analysis with Boundary Elements*, *144* (2022), Nov., pp. 185-198
[2] Tan, F., *et al*., The 2-D Numerical Manifold Method for Heat Conduction Problems, *Engineering Analysis with Boundary Elements*, *137* (2022), Apr., pp. 119-138
[3] Zhang, J. J., *et al*., Modelling and Prediction of Cutting Temperature in the Machining of H13 Hard Steel of Transient Heat Conduction, *Materials*, *14* (2021), 12, 3176
[4] Guo, L. Y., *et al*., Effect of Transient Thermal Conditions on Columnar-to-Equiaxed Transition during Laser Welding: A Phase-Field Study, *Metals*, *12* (2022), 4, 571
[5] Li, C., *et al*., Thermal Behavior and Flow Instabilities during Transient Chilldown of Liquid Rocket Engine by-Passive Re-Circulation Approach, *Cryogenics*, *99* (2019), Apr., pp. 87-98
[6] Fu, Z. J., *et al*., A Boundary Collocation Method for Anomalous Heat Conduction Analysis in Functionally Graded Materials, *Computers and Mathematics with Applications*, *88* (2021), Apr., pp. 91-109
[7] Jiang, G. H., *et al*., Shape Reconstruction in Transient Heat Conduction Problems Based on Radial Integration Boundary Element Method, *International Journal of Heat and Mass Transfer*, *191* (2022), Aug., 122830
[8] Yu, B., *et al*., The IG-DRBEM of 3-D Transient Heat Conduction Problems, *Engineering Analysis with Boundary Elements*, *128* (2021), Jul., pp. 298-309
[9] Yu, B., *et al*., The 3-D Transient Heat Conduction Problems in FGM Via IG-DRBEM, *Computer Methods in Applied Mechanics and Engineering*, *384* (2021), Oct., 113958

[10] Jacinto, C. C., *et al*., Coupling the BEM and Analytical Solutions for the Numerical Simulation of Transient Heat Conduction in a Heterogeneous Solid Medium, *Engineering Analysis with Boundary Elements*, *124* (2021), Mar., pp. 110-123
[11] Xu, C., *et al*., The RI-IGABEM Based on PIM in Transient Heat Conduction Problems of FGM, *Computer Methods in Applied Mechanics and Engineering*, *374* (2021), Feb., 113601
[12] Burgess, G., Mahajerin, E., A Comparison of the Boundary Element and Superposition Methods, *Computers and Structures*, *19* (1984), 5-6, pp. 697-705
[13] Sun H. C., *et al*., *Non-Singularity Boundary Element Methods* (in Chinese), Dalian University of Technology Press, Dalian, China, 1999
[14] Xu, Q., Sun, H. C., Unified Way for Dealing with 3-D Problems of Solid Elasticity, *Applied Mathematics and Mechanics-English Edition*, *22* (2001), 12, pp. 1357-1367
[15] Yang, D. S., Xu, Q., Virtual Boundary Meshless Least Square Integral Method with Moving Least Squares Approximation for 2-D Elastic Problem, *Engineering Analysis with Boundary Elements, 37* (2013), 3, pp. 616-623
[16] Yang, D. S., Ling, J., Calculating the Single-Domain Heat Conduction with Heat Source Problem by Virtual Boundary Meshfree Galerkin Method, *International Journal of Heat and Mass Transfer*, *92* (2016), Jan., pp. 610-616
[17] Yu, B., Yao, W. A., A Precise Time-Domain Expanding Boundary-Element Method for Solving 3d Transient Heat Conduction Problems with Variable Thermal Conductivity, Numerical Heat Transfer Part B, *Fundamentals*, *66* (2014), 5, pp. 422-445
[18] Yang, K., Gao, X. W., Radial Integration Bem for Transient Heat Conduction Problems, *Engineering Analysis with Boundary Elements*, *34* (2010), 6, pp. 557-563
[19] Ren, J. L., Xu, K., *et al*., Numerical Study of the 3d Variable Coefficient Heat Transfer Problem by Using the Finite Pointset Method, *Arabian Journal for Science and Engineering*, *46* (2021), 4, Apr., pp. 3483-3502

Paper submitted: February 15, 2023
Paper revised: April 19, 2023
Paper accepted: April 22, 2023